This is the peer reviewed version of the following article:
Ágnes Fiser-Nagy, Ilona Varga-Tóth, Tivadar M. Tóth (2014): Lithology identification using open-hole well-log data in the metamorphic Kiskunhalas-NE hydrocarbon reservoir, South Hungary.
Acta Geodaetica et Geophysica, March 2014, Volume 49, Issue 1, pp 57-78.
DOI: 10.1007/s40328-013-0037-1
The final publication is available at Springer via: http://dx.doi.org/10.1007/s40328-013-0037-1

Lithology identification using open-hole well-log data in the metamorphic Kiskunhalas-NE hydrocarbon reservoir, South Hungary

Ágnes Fiser-Nagy[1], Ilona Varga-Tóth[2], Tivadar M. Tóth[1]

[1]Department of Mineralogy Geochemistry and Petrology, University of Szeged, Szeged, Hungary
agnes.nagy@geo.u-szeged.hu; mtoth@geo.u-szeged.hu
[2]MOL Hungarian Oil and Gas Company; Budapest, Hungary
tvargane@mol.hu

Abstract
There are four main rock types along the ideal rock column of the Kiskunhalas-NE field; in order from the bottom upwards, orthogneiss, orthogneiss mylonite, graphitic gneiss mylonite and graphitic carbonate phyllite. These main rock types are characterized by significantly different reservoir features, as was proved by previous rock mechanical investigation. The geophysical information of well-logs (gamma, resistivity, neutron, density and acoustic logs) allows an understanding of the spatial extension of the good reservoir blocks. In the course of the examination conventionally applied plots, MN plots and discriminant function analysis were used. Three rock types were successfully identified along the wells, the graphitic carbonate phyllite, the mylonite and the orthogneiss. On the basis of the results, lithological boundaries could be estimated in numerous wells. These boundaries were presented along geological sections. Taking also the independent hydraulic regimes of the reservoir into account, a series of south-dipping normal fault-bounded blocks are assumed. Inside each block shallow-dipping mylonite/gneiss boundaries with a north-northeast dip direction are typical. The existence of this low-angled (less than 5°) mylonitized zone refers to a presence of a one-time detachment fault linked to the formation of a metamorphic core complex.

Keywords: lithology identification, porosity logs, MN plot, discriminant analysis,

1. Introduction

Fluid production from a fractured hard rock reservoir with heterogeneous petrological build-up is a real challenge. Hydrodynamic features of the reservoir may differ significantly for diverse rock types, because of their various rheological behaviours. In certain cases, not only lithology, but also spatial position of rock bodies with considerable internal structures (bedding, foliation, etc.), may play a role in the resulting brittle deformation. In fact, the spatial relationship between the directions of the rock structures and the brittle stress field is crucial. All lithological and structural features may finally define the hydrodynamic characteristics of the reservoir, which commonly exhibits a strongly compartmentalized

nature (e.g.: McNaugthon and Grab 1975, Árkai 1993, Aguilera 1995, Salah and Alsharhan 1998, Nelson 2001).

The study area of this research is the Kiskunhalas-NE (KIHA-NE) fractured metamorphic basement reservoir from the southern part of the Pannonian Basin. Previous studies (Nagy et al. 2013) showed that the four basic rock types of this basement high behave in a remarkably different way in the brittle field, causing diverse fracture geometries. While various mylonitic rock types tend to produce a dense fracture network, orthogneiss is free from communicating fracture systems. Bearing also in mind that, in the KIHA-NE field at present, not less than ten independent domains are defined hydrodynamically, a complicated mosaic of differently fractured rock bodies must be considered. In order to better understand the spatial relation of different rock types that tend to provide good reservoir qualities, a lithological framework should be put together. While the role of borecores is essential in petrological and petrophysical characterization, due to their very limited number well-logs must also be involved to spatially extend the information.

The aim of the present study is to maximize petrological and well-log information so as to construct a reliable framework of all rock types which have a bearing on the KIHA-NE reservoir.

2. Geological settings

The basement of the highly fragmented Pannonian Basin consists of microplates of diverse origins. The rather complex structural evolution of the region started with the less known Variscan orogeny (Szederkényi 1984, Árkai et al. 1985 Lelkes-Felvári et al. 2003, Lelkes-Felvári & Frank 2006), followed by an extensive extension, known as the Jurassic (Csontos et al. 1992, Haas & Péró 2004) and then the nappe formation in the Cretaceous (Rozlozsnik 1936, Ianovici et al. 1976, Bleahu et al. 1994, Német-Varga 1983, Tari et al. 1999). As a result of the complicated subsidence history during the Neogene (eg. Tari et al. 1992, Horváth 1995, Csontos & Nagymarosi 1998, Horváth et al. 2006), even more kilometre-deep sub-basins (Békés Basin, Makó Trench) and metamorphic highs, covered with just a few-hundred-metre-thick sediment (eg. Jánoshalma Dome, Szeghalom Dome), were formed (*Fig. 1a*). The so formed varied topographic and structural setup of the basement significantly affect the fluid flow system of the basin (eg. Vass et al. 2009); therefore, knowledge of them is essential, especially with respect to the production of the industrially important fluids, like thermal water and hydrocarbons.

The KIHA-NE fractured metamorphic hydrocarbon-reservoir is situated inside the Tisza Unit, NE from the Jánoshalma Dome and southwest from the Tázlár field (*Fig. 1a*). The 69 wells of the field reach the metamorphic basement at 1800–2000 m deep and generally penetrated to tens or even hundreds of metres. The previous papers (T. Kovács 1973, Árkai 1978, Cserepes 1980, T. Kovács & Kurucz 1984, Cserepes-Meszéna 1986, Árkai 1993) dealing with the field outline a diverse petrological build-up and various developments.

According to Nagy and M. Tóth (2012) four main rock types in the metamorphic basement of KIHA-NE were identified. On the basis of neighbourhood relations, these types define the following ideal rock column (*Fig. 1b*) from the bottom upwards. In the lowermost structural position, an orthogneiss with amphibolite xenoliths is common. On the basis of the petrological characteristics it is similar to the orthogneiss body of the neighbouring Jánoshalma Dome (T_1 ~ 700–850 °C, P_1 <0.65 GPa and T_2 < 580 °C, Zachar and M. Tóth 2004). The next lithology unit upwards is the mylonitized orthogneiss, which clearly differs from the next graphitic gneiss mylonite type in its mineral assemblage. The extensional fabric elements (C/S fabric, apatite bookshelf, boudinaged clasts and deformed quartz grains) are common in both mylonite types. Árkai (1978, 1993) was the first who recognized mylonitization of gneisses and mica schists in the studied region. In accordance with the quartz suture thermometer (Kruhl and Nega 1996), the temperature of the deformation event of these two mylonite types is estimated as T_{def} ~455 °C and the metamorphic temperature of the graphitic gneiss mylonite is T ~ 410 ± 45 °C using a carbonaceous material thermometer by Raman microspectroscopy (Beyssac et al. 2002, Rahl et al. 2005, Ayoa et al. 2010). The uppermost member of the ideal rock column, a graphitic carbonate phyllite (Árkai 1978, 1993), occurs only in a limited area of the site. Its carbonaceous material thermometer results suggest a T ~ 370 ±15 °C. In accordance with the previous and more recent results that there is approximately 200 °C diffreence in characteristic metamoprhic temperatures between the bottom (orthogneiss) and top (graphitic carbonate phyllite). The evolution of the two extreme rock bodies is significantly different and they were probably juxtaposed along an extensional shear zone (Nagy and M. Tóth 2012).

3. Methods

There is no outcrop in the basement; we only have information from several wells, penetrating the metamorphic mass around 100 m deep. Because of the limited sources of

information, we have to involve all data from the wells; the drilling documentation, the borecore samples and cuttings, as well as the well-logs; as follows (*Fig. 2*).

3.1 Drilling documentation

Drilling documentation serves the primary information about a well; it follows the "life" of the well from planning to closure. The daily report provides essential information on the presence and the extension of the lithotypes in the intervals without borecores. The lithotypes and the depths of the lithotype changes were determined primarily on the basis of cuttings. Nevertheless, detailed petrographic examination could not be carried out based on the on-the-spot cuttings because of their small size and the short time available for description. Therefore, the lithological classification at the well site is restricted to the macroscopically obvious differences.

3.2 Lithological classification

Accurate petrological information can be achieved only at the points of the borecores. In the borecores with conventional petrographic investigation (macro- and microscopic examination) the mineralogical composition, textural characteristics, and the extent of deformation could be established. On the basis of these characteristics, we can identify the different rock types of the field. Estimation of the (thermo- and barometric) metamorphic pathway helps in understanding the genetic relationship between the separated lithotypes that allow the definition of the (approximate) order in the ideal rock column. Even so, our lithological knowledge is limited to the sporadic borecores.

3.3 Well-log data evaluation

The several-decade-old well-logs were digitalized and only the good quality borehole logs were selected. If necessary, correction was applied to the logs. As only the metamorphic basement was the object of the present study, only these intervals were examined, the other sections were cut off. Most of the wells with good quality well-logs do not contain a borecore, thus we could not apply a direct borecore–log dataset. Instead, only the results of the petrological descriptions of the identified lithotypes and their ideal sequence along the rock column were considered.

On the digital data of the geophysical measurements, two-log (cross plots) and multi-log (MN plot) quantifications were computed, in order to group the log values and identify the

known lithotypes. Further statistical investigations (discriminant function analysis) were fulfilled to find the best separation algorithm between the lithology units. Furthermore, to estimate the rock type boundaries, the "predicted group" option of discriminant function analysis was used.

Cross plot is a simple graphical method to solve fairly complex relationships using two (or three) geophysical measurements; it can help to estimate the formation lithology. It has a general format; one measurement is displayed along the x-axis and another is displayed along the y-axis (Asyuith and Krygowsky 2004). The third measurement can be plotted with a colour scale. We can group the well-log values to define fields, also taking into account the depth of the data points, and relations between the two variables (Riden 1996, Steckham and Sauer 2010).

MN plot is a multi-log quantification; it combines the data of all three porosity logs to provide the lithology-dependent quantities *M* and *N*. *M* and *N* are simply the slopes of the individual lithology lines on the sonic-density and density-neutron cross plot charts, respectively. Thus, *M* and *N* are essentially independent of porosity and a cross plot provides lithological identification (Schlumberger 1989). M and N are defined as:

$$M = (\Delta t_{fl} - \Delta t) / (\rho_b - \rho_{fl}) \times 0.01 \text{ (x 0.03 metric)} \quad (1)$$

$$N = (\varphi_{Nfl} - \varphi_N) / (\rho_b - \rho_{fl}) \quad (2)$$

where Δt is the interval transit time in the formation (from the log), Δt_{fl} the interval transit time in the fluid in the formation, ρ_b the formation bulk density (from the log), ρ_{fl} fluid density in the formation, φ_N neutron porosity (from the log), φ_{Nfl} neutron porosity of the fluid of the formation (usually = 1.0). A number of common mineral points are plotted on the MN plot; conventionally this defines the limestone-sandstone-anhydrite-dolomite quadrangle (Asyuith and Krygowsky 2004), which are the common (sedimentary) reservoir lithologies. Although, in this case, the KIHA-NE reservoir is a metamorphic hard rock reservoir, this conventional quadrangle was used to facilitate the primary orientation inside the *MN* plots.

Discriminant function analysis is a suitable statistical method of assigning lithotypes to the log values; its task is to find the class, among those currently available, and that which most closely matches each unclassified sample. Therefore, this calculation requires *a priori* knowledge of classes (Benaouda et al. 1999). We aim to find the best separations in the datasets and estimate or evaluate the boundaries among the lithotypes along the wells.

3.4 The available open-hole well-logs

The *gamma* (*GR) log*, a measurement of the natural radioactivity of the formations, derives from ^{40}K, ^{238}U, ^{232}Th and their daughter elements. Out of these isotopes, the potassium content related mostly to clay minerals and potassium feldspar has a dominant role in a non-radioactive formation (Schlumberger 1989).

Because dry rocks are good electrical insulators, the *resistivity log (RT)* shows the fluid in the pores of the formations or absorbed in their interstitial clay. The resistance of a formation depends on the amount and the resistivity of formation water and the pore structure geometry (Schlumberger 1989). Each formation without fluids could have a different resistivity because of the different amount of included conductive minerals. The resistivity log is on logarithmic scale, unlike the others; therefore, the following transformation commonly used in the case of metamorphic rocks, was applied to them.

$$GYRT = 1 / \sqrt{RT} \quad (3)$$

The *sonic log* measures interval transit time (*Δt or DT*) of a compressional sound wave travelling through the formation along the axis of the borehole (Asyuith & Krygowsky 2004). In the simplest form, a sonic tool consists of a transmitter that emits a sound pulse and a receiver that picks up and records the pulse as it passes the receiver. Porosity decreases the velocity of the sound through the rock material and, correspondingly, increases the interval transit time. The interval transit time for a given formation depends on its lithology and porosity (Schlumberger 1989).

The *density log* measures the matrix density and the density of the fluid in the pores (Asyuith & Krygowsky 2004). A radioactive source applied to the borehole wall emits gamma rays into the formation (Schlumberger 1989). When the emitted gamma rays collide with electrons in the formation, the collisions result in a loss of energy from the gamma ray particle. The scattered gamma rays returned to the detectors in the tool measured on high energy range, are proportional to the electron density of the formation. In most rock types of interest in hydrocarbon exploration, the electron density is related to the formation true bulk density (ρ_b) through a constant (Tittman & Wahl 1965). The formation bulk density is a function of matrix density, porosity and density of the fluid filling the pores (Asyuith & Krygowsky 2004).

Neutron logs (φ_N) respond primarily to the hydrogen concentration in a formation. In a shale-free porous formation, where pores are filled with water or oil, the neutron log reflects the liquid filled porosity. Neutrons are created from a chemical source in the neutron logging

tool. These neutrons collide with nuclei of the formations and with each collision the neutron loses some of its energy. With enough collision, the neutron is absorbed by a nuclei and a gamma ray is emitted. Because the hydrogen atom is almost equal in mass to the neutron, maximum energy loss is dominated by a hydrogen atom. Therefore, the energy loss is dominated by the hydrogen concentration of the formation. The neutron log responses depend on the detector type and the lithology (Asyuith & Krygowsky 2004, Schlumberger 1989).

As, in this case, the porosity of the known basement lithologies of the investigated area is rather low, the porosity logs practically respond to the lithology features.

4. Data

4.1 Drilling documentation

In the basement of the KIHA-NE field, the daily reports separate two different rock types on the basis of cuttings; the graphitic carbonate phyllite and some kind of gneiss (*Fig. 2*). Due to the rather characteristic appearance of the graphitic carbonate phyllite (black colour), its location and the exact extension are well documented in the whole area.

4.2 Petrological information

The lithological classification and detailed petrographical description of the lithological units of Nagy and M. Tóth (2012) were used in the course of the present examination.

The *orthogneiss* of the KIHA-NE area consists of unweathered feldspar and quartz, and various amounts of biotite and muscovite flakes determine the slight foliation. Moderate weathering is present only in some places in the samples, while along the small number of narrow cracks small-scale alteration zones are common. There are a few amphibolite xenoliths and mica-poor granite dykes intercalated in the orthogneiss body (*Fig. 1b*).

The mineral assemblage and fabric elements (myrmekitic feldspar grains) of the *orthogneiss mylonites* suggest the relation to the orthogneiss underneath. The protolith orthogneiss underwent a strong shearing effect. As a consequence, the feldspars were sericitized, the biotite altered to chlorite, while mylonitic (C/S) foliation developed. A moderate amount of fractures and cracks is characteristic without any alteration zone and considerable open pore space in the orthogneiss mylonite rock body does not exist (*Fig. 1b*).

In the case of the *graphitic gneiss mylonite*, the intensive sericitization, the C/S foliation and mylonitic fabric elements are the same as in the orthogneiss mylonite samples. However, the absence of biotite and/or chlorite, and the presence of graphite and sulphide minerals as

index phases, clearly separate this block from the underlying orthogneiss mylonite. The samples are commonly fractured and oil spotted, containing significant open pore spaces (*Fig. 1b*).

On the top of the basement, the mostly chaotically folded *graphitic carbonate phyllite* appears. In this low grade metamorphic rock, black bands alternate with white bands (*Fig. 1b*). The major rock forming minerals are graphite (black bands), carbonate and white mica (white bands), with subordinates containing sulphide minerals and some quartz too. The mylonitic features are absent; nevertheless, extensional fabric elements (pressure fringes around pyrite cubes) are characteristic of its texture.

4.3 Well-logs

As mentioned above, the only geophysical data available in the KIHA-NE field are the several-decade-old digitalized well-logs; a seismic section does not pass through the investigated area. Fifteen out of the total of 69 wells have invaluable well-logs with porosity logs. Altogether, nine wells have all three porosity logs, five of them have two porosity logs without any borecores, and one has only the neutron log, but it also has borecores. Further four wells, with only the gamma and resistivity logs, were used in the course of the evaluation because of their lithologically various borecores (*Table 1*).

5. Results and discussion

5.1 Separation and identification of the orthogneiss and the mylonitic lithologies

First, let us look at those wells, which, according to the cuttings, did not contain graphitic carbonate phyllite. Consequently, the “gneissic” lithology of the field notes could be identified as one of the remaining three rock types (mylonites and orthogneiss). There are some wells with a limited porosity log range, but which have numerous borecores from the gneiss and some from the mylonitic rock types. In the case of Well-Q, there are several borecores belonging to the orthogneiss and its mylonitic variety. On the plot of gamma-resistivity, the data points of its borecores (the coloured circles) appear separately (*Fig. 3a*), and the further values are grouped around them. The points around the gneiss mylonite belong to the upper section of the well, while the other group, around the gneiss borecore data points, belongs to the lower section of the well. The mylonitic interval is characterized by higher gamma values and lower resistivity than those typical of the gneiss group.

In Well-J, according to the numerous borecores, three lithotypes are represented; graphitic gneiss mylonite, orthogneiss mylonite and orthogneiss. Even so, on its gamma-resistivity cross plot, just two groups exist (*Fig. 3b*); the datapoints of the orthogneiss samples are separated from the mylonitic samples. The graphitic gneiss mylonite and the orthogneiss mylonite borecore values appear as overlapping groups; thus, despite the clear petrological difference, the two mylonitic lithotypes do not deviate in a well-log sense. The result of Well-I corroborates that the mylonitic lithologies of KIHA-NE are not separable in a well-logging way, since its graphitic gneiss mylonite and orthogneiss mylonite borecores do not deviate on its cross plots. In Well-J, the log values of the short interval without borecores coincide with the orthogneiss group, confirming the suggested identification by their depth. The group of mylontic lithotypes presents with higher gamma values compared with the orthogneiss datapoints.

Eight wells have all porosity logs, but without any available borecores. In these cases, all the porosity logs were plotted with each other in every possible variation in all cases. The points of all the wells suggest the existence of diverse groups in these diagrams. The best separation is shown by Well-F, where the two groups clearly appear on each plot, being the most spectacular on the density-sonic plot (*Fig. 3c*). Furthermore, samples of these groups cluster separately along the well; the upper section of the well is characterized by lower density and higher Δt compared to the lower section. Nevertheless, the two separated intervals of the well do not show any noticeable deviation in gamma values.

The lithology sensitive MN plot needs all three porosity logs, so it was completed only for those wells with all of them. To assist the orientation on the MN plot, merely for the sake of simplicity, the conventionally used quadrangle of anhydrite (A) – sandstone (S) – limestone (L) – dolomite (D) was used. The obtained MN plots generally show two groups with varied standard deviations, and, in some cases, only one of the groups is present. The best example to exhibit the strength of the MN plot is Well-F (*Fig. 3d*), where both groups exist separately. The upper section of the well is represented by points along the lower side (A–S) of the quadrangle, while the lower section of the well exists along the upper side (D–L). Two further separated groups appear on this plot; namely the data points of the potassium feldspar-rich intervals (*Fig. 3d*) and the calcium and sodium feldspar-rich intervals (*Fig. 3d*). These short intervals are dispersed along the well.

The two groups of the MN plot along the lower and the upper sides of the quadrangle coincide with the groups separated in the cross plots previously (*Fig. 3c*). The upper interval

of the well is characterized by lower density and higher sonic values compared to the underneath section. This could mean that the upper interval is looser and has higher mica content; the latter also is responsible for higher gamma values (*Fig. 3a, b*). These features together with considering the ideal sequence along the rock column (*Fig. 1b*), suggest that the group along the A–S side of the quadrangle belongs to the mylonitic rock types. Because of shearing and its attendant alteration process, the mylonitic zones are looser and are richer in micas than the non-deformed orthogneiss body. As a result, the other group along the D–L side of the quadrangle is identified as the orthogneiss lithology. There are some cases where only one of these groups appears on the MN plot; in these wells just one lithology is represented along the whole well. Although, Árkai (1993) proved the significant role of ancient chemical and physical weathering at the top of the metamorphic basement, here higher gamma values and the lower density are characteristic physical features of the mylonites and do not necessarily indicate surface processes.

5.2 Estimation of the boundary between orthogneiss and mylonitic lithologies

After the separation and identification of the gneiss and mylonite lithotypes, we would like to know which well-log measurements and the extent to which the separation between the two lithologies are defined. For this purpose, discriminant function analysis was carried out. In the first step, all porosity log data of Well-F were used with the aim of defining the function which best separates the two lithologies. In the second step, this function can be applied to all other wells. As a result, the boundary between the separated lithology units can be estimated using the predicted membership values computed by discriminant analysis.

Figure 4a shows the histogram of the discriminant scores of Well-F with the two fairly well separated groups of mylonite and gneiss values. The higher discriminant score values concern the mylonite lithology, while the lower discriminant score values refer to orthogneiss. According to the discriminant function:

$$D(1)= (0.361*S +2.146*D + 5.393*R) – (0.389*N +26.297) \quad (4)$$

the dominant parameters in the separation are density (D) and resistivity (R) besides the neutron (N) and sonic (S) logs. In *Figure 4b* discriminant scores along the depth are present; the boundary between the two lithologies can be estimated at 2094.7 m on the basis of the predicted group membership values calculated for the D(1) discriminant function.

Afterwards, the D(1) function was applied for the remaining seven wells with all porosity logs. One example is demonstrated, the case of Well-D, in *Figure 4c, d*. The

resulting scores of D(1) are plotted with the depth (*Fig. 4d*); the upper section of the well belongs to the mylonite lithology and has higher discriminant score values compared to the lower interval of the borehole, that is, the non-deformed gneiss. This identification is confirmed by the MN plot results also, shown on *Figure 4c*. The boundary was estimated at 2100.8 m between the mylonite and the gneiss units. The extremely high values of the gneiss unit (*Fig. 4b, d*) might belong to narrow sheared zones, while the much lower score values inside the mylonite unit could represent less mylonitized bands, as the log features of these intervals are closer to that common for the gneiss type.

There are some wells without the whole range of porosity logs; either the density or the sonic is absent. Although, in these cases, the MN plot is unusable, the discriminant function analysis might be successful. Identically to the previous seven cases, the discriminant scores of the D(1) function consistently show that the mylonites have higher values (ca. > 0) and the orthogneiss have lower values (ca. ≤ 0). So, as the results of MN plots and discriminant analysis coincide, in all cases when the MN plot cannot be applied in the absence of any of the porosity logs, lithologies can be separated using the statistical approach alone. The previously efficiently used dataset of Well-F was used in the cases where one of the porosity logs is absent. At first, calculation without sonic measurements was carried out. In this case, the gneiss and mylonite zones of Well-F could well be separated (*Fig. 5a*) using the function of:

$$D(2) = (3.357*D + 33.337*R) – (0.208*N + 0.007G +11.157). \quad (5)$$

The resistivity (R) and the density (D) logs are the main parameters in the separation besides the neutron (N), while the gamma log (G) has a very low effect on it. The D(2) function was applied successfully on all wells with only density and neutron porosity and without sonic logs; the lithology and the boundary of all these wells could be estimated convincingly. As in the case of Well-N (*Fig. 5b*), the upper interval of the well is mylonite up to 2099.4 m, while further down orthogneiss is common.

In the other case, where the density log is missing and sonic and neutron are involved from the porosity logs, the discriminant analysis of Well-F produces the histogram in *Figure 5c*, where the separation of the mylonite and gneiss lithology is quite good, using the function of:

$$D(3)= (0.377*S) – (0.366*N +21.021). \quad (6)$$

But the application of the D(3) function for the wells does not work; in the example of Well-O the discriminant scores (*Fig. 5d*) do not show any pattern similar to the previous ones, neither

the identity of the lithologies nor the boundary between them could be established. Nonetheless, this experiment further confirms that, when separating gneiss and mylonite, the density measurement plays the major role (together with the resistivity), and the sonic log is not suitable.

Finally, Well-Q, with only the neutron measurements from the porosity logs, explores some borecore samples from both orthogneiss and its mylonite. According to the previous practice, the dataset of Well-F was the starting point of the discriminant function analysis. On the histogram of the discriminant scores (*Fig. 6a*) separation of the two lithologies is satisfactory using only the neutron, gamma and resistivity measurements; the function is:

$$D(4)= 30.834*R – (0.245*G + 2.714) \quad (7)$$

The main separating log is the resistivity (R), the gamma (G) log is subordinate, while the neutron (N) has no role. The D(4) function was applied on the dataset of Well-Q and the resulting discriminant scores along the depth are shown in *Figure 6b* with locations of the known borecores (coloured circles). The known intervals fit into the separated sections of mylonite and orthogneiss. The boundary between the two lithology units was estimated at a depth of 2081.7 m. There is an interval (without sample) around the 2160 m depth in the orthogneiss unit, with consistently higher discriminant score values; this might be a sheared zone inside the otherwise non-deformed orthogneiss unit.

Finally, discriminant analysis was carried out on the dataset of Well-Q too in order to check whether the D(5) function works satisfactorily on the dataset of Well-F. The discriminant scores of Well-Q appear with quite good separation (*Fig. 6c*), with the function of:

$$D(5) = (11.035*R + 2.580*N + 0.081*G) – 13.107 \quad (8)$$

Similar to D(4), the most dominant measurement is the resistivity (R); but the neutron log (N) has a greater role than the gamma (G), contrary to *Equation 7*. The plot of the discriminant scores of Well-F by *Equation 8* are presented in *Figure 6d*. The previously identified lithologies (*Fig. 3a, b, Fig. 4a, b*) are indicated in it. Although the separation is not as adequate, it is clear that the upper section of the well has higher discriminant score values than the lower. Thus, the previously identified lithologies on the MN plot are proved by a direct link with the exactly known borecores of Well-Q.

5.3 Separation and boundary estimation between graphitic carbonate phyllite and mylonitic lithologies

Look at the wells that, according to the cuttings, explore the graphitic carbonate phyllite lithology. In Well-R, all the porosity logs are available and the upper section of the explored rock column belongs to the graphitic carbonate phyllite. The cross plots of the porosity measurements of the well show two slightly separate groups, presented on the density-neutron plot (*Fig. 7a*). The graphitic carbonate phyllite values have a higher standard deviation in the neutron measurements, compared to the remaining "some gneiss" section. On the gamma-resistivity plot (*Fig. 7b*) the extremely low resistivity values of the graphitic carbonate phyllite are conspicuous. Furthermore, its gamma measurements clearly show lower values than those characteristic of the "some gneiss" unit. Well-S has some graphitic carbonate phyllite and graphitic gneiss mylonite borecores, but does not have any porosity logs. Its gamma-resistivity plot shows a rather similar sight to the case of Well-R (*Fig. 7b)*; the borecores of graphitic carbonate phyllite appear with high standard deviation in the low resistivity field, while the mylonitic borecores and the remaining intervals of the well have higher resistivity and gamma values.

On the MN plot, the known graphitic carbonate phyllite and the remaining values are aligned with the lower side (A–S) of the anhydrite (A) – sandstone (S) – limestone (L) – dolomite (D) quadrangle. This position, according to the orthogneiss vs. mylonite MN plots (*Fig. 3b*, *Fig. 4*c), suggests that the "some gneiss" lithology in this well should be the mylonitic lithology. The gamma-resistivity plot of Well-S is also confirmed.

Discriminant function analysis was fulfilled for these two lithologies (graphitic carbonate phyllite and mylonite) on Well-R. The result shows a fairly good separation (*Fig. 7d*), using the function of:

$$D(6)= (0.021*S + 0.474*N +1.824*D + 7.348*R) – (0.059*G + 4.229). \quad (9)$$

Besides, the resistivity (R), the density (D) and neutron (N) measurements have the main role in the separation, while the sonic (S) and the gamma (G) logs are subordinate. The boundary between the two rock units is estimated at 2061 m. This depth coincides well with the noted boundary in the drilling documentation. As none of the other wells that contain graphitic carbonate phyllite have porosity logs, further application of the D(6) function is not possible.

5.4 Spatial extension of the estimated lithological boundaries

There is insufficient data to construct an entire 3D rockwork model for the whole study area; nevertheless, along certain geological sections it is possible to extend information in 2D. Neighbouring wells were used with a mylonite/gneiss boundary along two lines, which pass

through the field (*Figs. 8, 9*). These sections could provide information about the structural build-up of the area. In the course of the interpretation of the sections we took into consideration the ten known hydraulic regimes in the field (unpublished industry report, *Fig. 8*). Within each regime, all wells communicate with each other, but have no hydraulic connectivity with any other well outside that sub-area. Such communication among the wells might be in relation to the structural geometry of the field. As common examples, impermeable fault zones or even unfractured rock masses may define regime boundaries.

Along the AB section (*Fig. 9*) the two regime boundaries could be interpreted as normal faults with a southern dip. The mylonite/gneiss boundaries inside all the three regimes have a very similar, moderate northern dip. Along the AC section (*Fig. 9*) one of the regime boundaries could be interpreted as a normal fault (as in the case of the AB section); the mylonite/gneiss boundaries inside both separated blocks have a moderate northern dip as well. Inside the northern block along the AC section, three independent hydraulic regimes exist (*Fig. 8*), but there is no indication of the presence of additional normal faults. Consequently, there should be another factor responsible for separation inside the hydraulic system. Although the well-logs record it as a homogenous block, it is known from the previous petrological studies that the mylonite is petrologically extremely heterogeneous. The two different mylonite types exhibit different reservoir features; so the orthogneiss mylonite samples have a small amount of natural fractures and, according to the previous rock mechanical tests (Nagy et al. 2013), this block is characterized by moderate anisotropy and tendency to fracture. In this body, formation of a complicated and connected fracture system is unlikely. The graphitic gneiss mylonite block contains strongly fractured, locally brecciated, and oil spotted borecore samples. Rock mechanical tests pointed out that a possible communicating fracture system can be achieved by much lower amount of invested work than for other lithologies. Furthermore, these tests clearly indicate that the orientation of the mylonitic foliation also has a significant influence on the reservoir features; the graphitic gneiss mylonite samples show high anisotropy depending on the sample orientation in the compressive test. A remarkable difference can be computed between the samples tested parallel and perpendicular to the preserved foliation of the rock (Nagy et al. 2013). Therefore, we could assume that, in addition to post-metamorphic, impermeable fault zones also change in petrographic characteristics and that orientation of the main structures inside the blocks with different lithologies determine the hydraulic behaviour of the field.

The eminent role of the mylonite zone in the behaviour of the whole fractured reservoir is also proved by the positions of hydrocarbon productive intervals. As is indicated in *Figure 9*, in each case where a restricted productive interval can be localized, the hydrocarbon production clearly comes from the mylonitized zone. In the other cases, the perforation covered a significant interval of the wells involving also the lowermost orthogneiss. In fact, almost the whole depth of these wells is open for fluid flow and there is no way to point the most productive intervals. Nevertheless, also keeping in mind the rock mechanical data, one can suppose that the main productive zones, even in these cases, can be linked to mylonitic horizons. The overlying Miocene limestone is also productive for hydrocarbon in certain wells, clearly proving hydrodynamic communication between the fractured basement reservoir and the sedimentary cover.

Inside each fault-bounded regime, the orientation (dip and dip angle) of the mylonite/gneiss boundary surface could be calculated, if more than two data points exist. According to three independent calculations, this dip direction is rather consequent, being north-northeast (13°–18°), and the angle is systematically less than 5°. So the investigated KIHA-NE area is characterized by a shallow-dipping extensional mylonite zone. This wide zone separates blocks of systematically different metamorphic evolution and peak conditions. Formation of such a shear zone is typical when metamorphic core complexes develop during continental extension along low-angle (<30°) detachment faults (Lister & Davis 1989). Mylonitic gneiss formation at several-kilometre depths along major shallow-dipping ductile shear zones is linked to activity of these detachment faults. The detachment faults usually form at the beginning of the extension process; however, they do not remain active throughout the entire geological history of the metamorphic core complex (Lister & Davis 1989). Later, when these mylonitized zones uplift and deform in the brittle deformation zone, they may be overprinted by cataclasis of brecciation (Lister & Davis 1989) or even become fragmented along normal faults of younger tectonic movements.

In numerous fields the incompatible rock column is accompanied by sheared lithologies (e.g., Mezősas-Furta – M. Tóth and Zachar 2006, Szeghalom – Schubert and M. Tóth 2001, Jánoshalma – Zachar and M. Tóth 2004, Dorozsma – M. Tóth et al. 2002, Kiskunhalas – Nagy and M. Tóth 2012), suggesting that the current order of rock units was created by post-metamorphic tectonic movements. Unfortunately, just a little information and data is available in publications and industrial reports about the physical condition and ages of these shear zones and there is no clear theory about the structural evolution of these horizons; rather,

there are many contradictory hypotheses (e.g., Lelkes-Felvári et al. 2005, Balogh et al. 2009, M. Tóth 2013).

After the Variscan ages there were several optional large scale tectonic events, which might have caused the development of the fault related rocks in the basement. The first detected metamorphic events of these orthogneiss happened during the Variscan orogeny (e.g., Szederkényi 1996, Kovács et al. 2000, Balogh et al., 2009), although the age constraints regarding the detailed metamorphic evolution is still rather limited. There are numerous 330 Ma and younger Variscan ages relating to different states of the complicated metamorphic history (e.g., Árkai et al. 1985, Szederkényi et al. 1991, Lelkes-Felvári et al 2003, 2005, Balogh et al. 2009). Regarding the Variscan uplift and the synchronous shear events only very poor data is available. In Szeghalom, a deformation age of the Permian (280.2 ± 10.5 Ma from mylonitic white mica, K/Ar age) is documented (M. Tóth 2013). In the Dorozsma basement, Dunkl (1994) provides an Early Triassic FT age, which refers to the age of its post-metamorphic uplift. The effect of the Jurassic continental rifting (Haas and Péró 2004) caused, for example, the coal formation of the Mecsek Mountains in half graben structures; this large scale extension event may have had a relationship with the Jurassic (186.9 ± 7.1 Ma feldspar K/Ar age; 160.2 ± 8.7 Ma zircon FT age) ages in the sheared metamorphic basement mentioned by Balogh et al. (2009). In the course of the Alpine orogeny (Cretaceous and younger) north vergent nappes (e.g., Codru nappe system) and slices formed inside the Tisza Unit (e.g., Rozlozsnik 1936, Német-Varga 1983, Tari 1999). Cretaceous ages (95.2±1.8 – 58.4±1.3 Ma; Ar/Ar muscovite ages; Lelkes-Felvári et al. 2005) were measured, among many others in metamorphic rocks of the Algyő complex. The Miocene back-arc basin extension related to the Alpine orogeny (Hajnal et al. 1996) generated a number of uplifted and tilted blocks and a set of pull-apart basins (Tari et al. 1992). Seismic measurements suggest uplifted metamorphic highs interpreted as metamorphic core complexes (Horváth et al. 2006). A series of subhorizontal reflections were detected in the basement around Szeghalom, related to this rather quick uplift (Posgay et al. 2006).

All these tectonic events may have caused wide tectonic zones (either mylonitic or cataclastic) and contributed to the development of the juxtaposed block with different metamorphic evolutions and ages inside the metamorphic basement.

6. Summary

On the basis of well-log data, basic lithologies of the KIHA-NE metamorphic basement high can be distinguished; we can separate orthogneiss from mylonite and mylonite from graphitic carbonate phyllite by using conventional plots (especially the MN plot) and a statistical approach (discriminant function analysis). In the separation algorithms, the density and resistivity logs have a major role. The lithologically different mylonitized rock types cannot be separated by these methods.

In the course of the spatial extension of the results, spatial positions of the independent hydraulic regimes can also be taken into account. On the resultant geological sections, several south-dipping normal fault-bounded blocks are assumed, which clearly record shallow-dipping mylonite/gneiss boundaries with a north-northeast dip direction. Existence of this low-angle mylonitized zone refers to the presence of a one-time detachment fault linked to the formation of a metamorphic core complex. Based on this structural image, the spatial position of the mylonite zone can be extended for the whole area. As mylonite is the only basement lithology that serves remarkable fractured porosity, the spatial model may contribute significantly to producing more accurate reservoir models.

Acknowledgements

We thank MOL Hungarian Oil and Gas Company for making the study of the open-hole well-logs possible. Balázs Kiss is thanked for the fruitful discussions about the behaviour of the KIHA-NE reservoir. Péter Árkai and István Kovács are thanked for the thorough review. This research was supported by the European Union and the State of Hungary, co-financed by the European Social Fund in the framework of TÁMOP 4.2.4. A/2-11-1-2012-0001 ‘National Excellence Program’. English was corrected by Proof-Reading-Service.com.

References

Aguilera R. (1995): Naturally fractured reservoirs. 2nd Edition. Penwell Publishing Company, Tulsa, Oklahoma.

Aoya M, Kouketsu Y, Endo S, Shimizu H, Mizukami T, Nakamura D, Wallis S (2010) Extending the applicability of the Raman carbonaceous-material geothermometer using data from contact metamorphic rocks. J Metamorph Geol 28(9):895–914.

Árkai P (1978) A Kiskunhalas ÉK-I terület mezozoikumnál idősebb metamorf és magmás képződményeinek szénhidrogénprognózist elősegítő ásványtan-kőzettani és geokémiai vizságlata. MTA GKI (Manuscript),

Árkai, P., Nagy, G., Dobosi, G. (1985): Polymetamorphic evolution of the South-Hungarian crystalline basement, Pannonian Basin: geothermometric and geobarometric data. - Acta Geol. Hung., 28, 165-190.

Árkai P (1993) The distinction between low-T retrograde metamorphism and weathering + burial diagenesis of the gneiss and mica schist basement complex, Great Plain, Hungary: A novel use of illite "crystallinity". Neues Jahrbuch für Mineralogie, Monatshefte, H. 8:337-351.

Asquith G, Krygowsky D (2004) Porosity Logs. In.: Basic Well Log Analysis: AAPG Methods in Exploraion 16:37-76.

Balogh K., M. Tóth T., Dunkl I., Scherrer N. (2009): A polimetamorf aljzat geokronológiai viszonyai a Szeghalom és a Mezősas-Furta háton. (Gechronology of the polymetamorphic basement in the Szeghalom and Mezősas-Furta highs.) In: M. Tóth, T. (ed.): Magmás és metamorf képződmények a Tiszai Egységben. GeoLitera, 147-160.

Benaouda D, Wadge G, Whitmarsh RB, Rothwell RG, Macleod C (1999) Inferring the lithology of borehole rocks by applying neural network classifiers to downhole logs: an example from the Ocean Drilling Program. Geophy. J. Int. 136:477-491.

Beyssac O, Goffé B, Chopin C, Rouzaud N (2002) Raman spectra of carbonaceous material in metasediments: a new geothermometer. J Metamorph Geol 20:859–871.

Bleahu M, Haas J, Kovács S, Péró Cs, Mantea G, Bordea S, Panin S, Bérczi-Makk A, Stefanescu M, Konrád Gy, Nagy E, Rálisch-Felgenhauer E, Sikic K, Török Á (1994) Triassic facies types evolution and paleogeographic relations of the Tisza megunit. Acta Geologicy Hungarica, 37:187-234.

Cserepes L (1980) A Duna-Tisza Közi karbonnál idősebb képződmények petrológiai vizsgálata MSZKFI, Budapest.

Cserepes-Meszéna B (1986): Petrography of the crystalline basement of the Danube-Tisza Interfluve (Hungary). Acta Geol Hung 29(3–4):321–339.

Csontos L, Nagymarosy A (1998) The Mid-Hungarian line: a zone of repeated tectonic inversions. Tectonophysics 297(1–4):51–71.

Csontos L, Nagymarosy A, Horváth F, Kovac M (1992) Tertiary evolution of the Intra-Carpathian area: a model. Tectonophysics 208:221–241.

Haas J, Péró Cs (2004) Mesozoic evolution of the Tisza Mega-unit. Int J Earth Sci 93(2):297–313

Haas J, Budai T, Csontos L, Fodor L, Konrád Gy (2010) Pre-Cenozoic geological map of Hungary, 1:500 000. Geological Institute of Hungary.

Hajnal Z., Reilkoff B., Posgay K., Hegedus E., Takacs E., Asudeh I., Mueller J. Ansorge R, DeIaco R. (1996): Crustal-scale extension in the central Pannonian basin. Tectonophysics, 264/1-4, 191-204.

Horváth F (1995) Phases of compression during the evolution of the Pannonian Basin and its bearing on hydrocarbon exploration. Mar Petroleum Geol 12(8):837–844.

Horváth F, Bada G, Szafián P, Tari G, Ádám A, Cloetingh S (2006) Formation and deformation of the Pannonian Basin: constraints from observational data. In: Gee DG, Stephenson RA (eds) European lithosphere dynamics. Geological Society, London, Memoirs 32:191–206.

Ianovici V, Borcos M, Bleahu R, Patrulius D, Lupu M, Dimitrescu R, Savu H (1976) La géologie des Monts Apuseni. Editions de Academi, Bucuresti.

Kovács S., Haas J., Császár G., Szederkényi T., Buda Gy., Nagymarosy A. (2000): Tectonostratigraphic terranes in the pre-Neogene basement of the Hungarian part of the Pannonian area. Acta Geol Hung 43, 225–328.

Kruhl JH, Nega M (1996) The fractal shape of sutured quartz grain boundaries: application as a geothermometer. Geol Rundsch 85:38–43.

Lelkes-Felvári Gy, Frank W, Schuster R (2003) Geochronological constraints of the Variscan, Permian–Triassic and eo-Alpine (Cretaceous) evolution of the Great Hungarian Plain basement. Geol Carpath 54(5):299–315.

Lelkes-Felvári Gy., Schuster R., Frank W., Sassi R. (2005): Metamorphic history of the Algyő High (Tisza Mega-unit, basement of Great Hungarian Plain) – a counterpart of crystalline units of the Koralpe-Wölz nappe system (Austroalpine, Eastern Alps). Acta Geologica Hungarica, 48/4, 371-394.

Lelkes-Felvári Gy, Frank W (2006): Geochronology of the metamorphic basement, Transdanubian part of the Tisza Mega-Unit. Acta Geol Hung 49(3):189–206

Lister GS, Davis GA (1989) The origin of metamorphic core complexes and detachment faults formed during Tertiary continental extension in the northern Colorado River region, U.S.A. J of Structural Geol 11(1/2):65-94.

M. Tóth T., Zachar J. (2006): Petrology and deformation history of the metamorphic basement in the Mezősas-Furta crystalline high (SE Hungary). Acta Geol. Hung., 49/2, 165-188.

M. Tóth T., Schubert F., Földes T., Hollós Cs., Komlósi J. (2002): Modelling of the fractured Dorozsma crystalline reservoir, SE Pannonian Basin. EAGE Annual Meeting Abstracts 297.

M. Tóth T. (2013): Evolution of the Körös Complex orthogneiss, Tisza Megaunit, SE Hungary. Submitted to Lithos.

McNaughton D. A., Garb F. A. (1975): Finding and Evaluating Petroleum Accumulations in Fractured Reservoir Rock. Exploration and Economics of the Petroleum Industry, 13, 45-54.

Nagy Á, M. Tóth T, (2012) Petrology and tectonic evolution of the Kiskunhalas-NE fractured CH-reservoir, S-Hungary. Central European Geology, 55(1):1–22.

Nagy Á, M. Tóth T, Vásárhelyi B, Földes T (2013) Integrated core study of a fractured metamorphic HC-reservoir; Kiskunhalas-NE, Pannonian Basin. Acta Geod Geophys. 48(1):53-75.

Nelson R. (2001): Geologic analysis of naturally fractured reservoirs. Gulf Professional Publishing.

Német-Varga Z (1983) Tectonics of the Mecsek Mountains in the Apline orogenic cycle. Annual Reposrt Hungary Geological Survey, 1981:467-484.

Posgay K., Bodoky T., Hajnal Z., M. Tóth T., Fancsik T., Hegedűs E., Cs. Kovács A., Takács E. (2006): Interpretation of subhorizontal crustal reflections by metamorphic and rheologic effects in the eastern part of the Pannonian Basin. Geophys. J. Int. 167, 187–203.

Rahl JM, Anderson KM, Brandon MT, Fassoluas C (2005) Raman spectroscopic carbonaceous material thermometry of low grade metamorphic rocks: Callibration and application to tectonic exhumation in Crete, Greece. Earth and Planetary Science Letters, 240(2):339–354.

Riden MH (1996) Lithology Reconstruction from logs. In: Geological Interpretation of Well Logs, 2nd Edition Whittles Publishing. 151-168.

Rozlozsnik P (1936) Die tektonische Stellung der bihargebirgsgruppe (Muntii Apuseni) im Karpatensystem. Math. und Naturwissenschaft, anzeiger Budapest, 55:6-76.

Salah M. G., Alsharhan A. S. (1998): The Precambrian basement: a major reservoir in the rifted basin, Gulf of Suez. Journal of Petroleum Science and Engineering, 19/3, 201-222.

Schlumberger (1989) Log Interpretation Principles/Applications. Schlumberger Wireline & Testing, Texas.

Schubert F., M. Tóth T. (2001): Structural evolution of mylonitized gneiss zone from the Norther flank of the Szeghalom dome (Pannonian Basin, SE, Hungary). Acta Min. Pet. Szeged, 42, 59–64.

Steckhan, J, Sauer R (2010) Introduction of a Rock Typing Methodology in Crystalline Basement Reservoirs (Yemen). Extended abstract of AAPG International Conference and Exhibition, Rio de Janeiro, Brazil, November 15-18, 2009

Szederkényi T (1984) Az Alföld kristályos aljzata és földtani kapcsolatai. DSc Thesis,

Szederkényi T. (1996): Metamorphic formations and their correlation in the Hungarian part of the Tisza Megaunit (Tisza Composite Terrane). Acta Min Petr Szeged 37, 143-160

Szederkényi T., Árkai P., Lelkes-Felvári Gy. (1991): Crystalline groundfloor of the Great Hungarian Plain and South Transdanubia. In: Karamata, S. (ed.): Geodynamic evolution of the Pannonian Basin, 261-273.

T. Kovács G (1973) A Duna–Tisza köze déli részének földtani fejlődés története (Geological evolution of the southern part of the Danube–Tisza Interfluve). PhD. Thesis, JATE, Szeged, Hungary.

T. Kovács G, Kurucz B (1984) A Dél-Alföld mezozoikumnál idősebb képződményei (Formations older than Mezozoic of the Southern Great Hungarian Plain). MÁFI, Budapest.

Tari G, Horvath F, Rumpler J, (1992) Styles of extension in the Pannonian Basin. Tectonophysics, 208(1-3):203-219.

Tari G, Dövényi P, Dunkl I, Horváth F, Lenkey L, Stefanescu M, Szafián P, Tóth T (1999) Lithospheric structure of the Pannonian basin derived from seismic, gravity and geothermal data. Geological Society, London, Special Publications; 156:215-250.

Tittman J, Wahl JS (1965) The physical foundations of formation density logging (gamma-gamma). Geophysics 30(2):284-294.

Vass I, M. Tóth T, Szanyi J, Kovács B (2009) Az aljzat kristályos hátának szerepe az Alföld fluidum áramlási és hőtransport folyamataiban. In.: M. Tóth T ed.: Igneous and metamorphic formations of the Tisza Unit. GeoLitera, 325-339.

Zachar J, M. Tóth T (2004) Petrology of the metamorphic basement of the Tisza Block at the Jánoshalma High, S Hungary. Acta Geologica Hungarica, 47(4):349-371.

Figures:

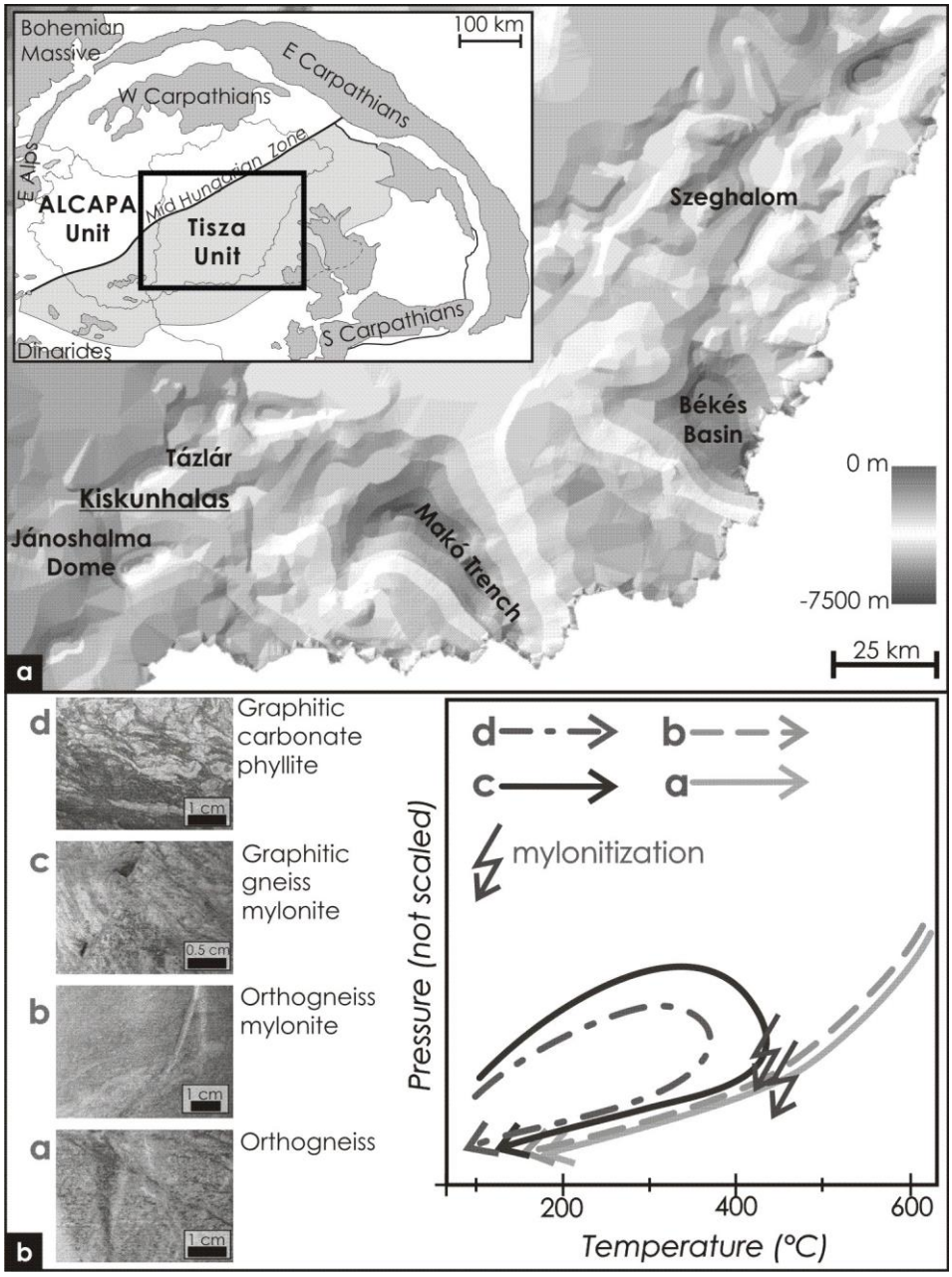

Figure 1. a) Location of the Kiskunhalas-NE field in the Pannonian Basin (After Haas et al. 2010). b) Representative macroscopic picture of the litotypes in the order of the ideal rock column and metamorphic evolution (with arrows) of them (after Nagy & M. Tóth, 2012) Legend: a – orthogneiss, b – orthogneiss mylonite, c – graphitic gneiss mylonite, d – graphitic carbonate phyllite.

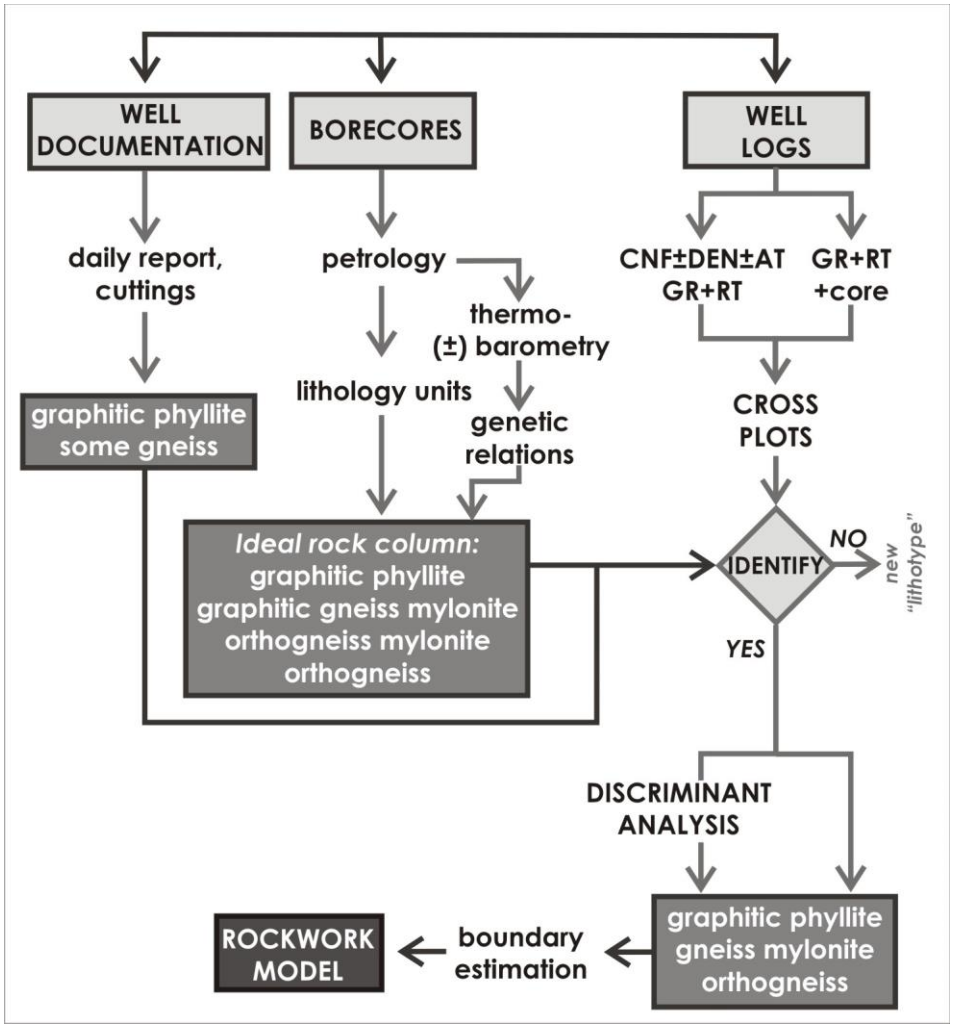

Figure 2. Flow chart of the methods (see further in the text).

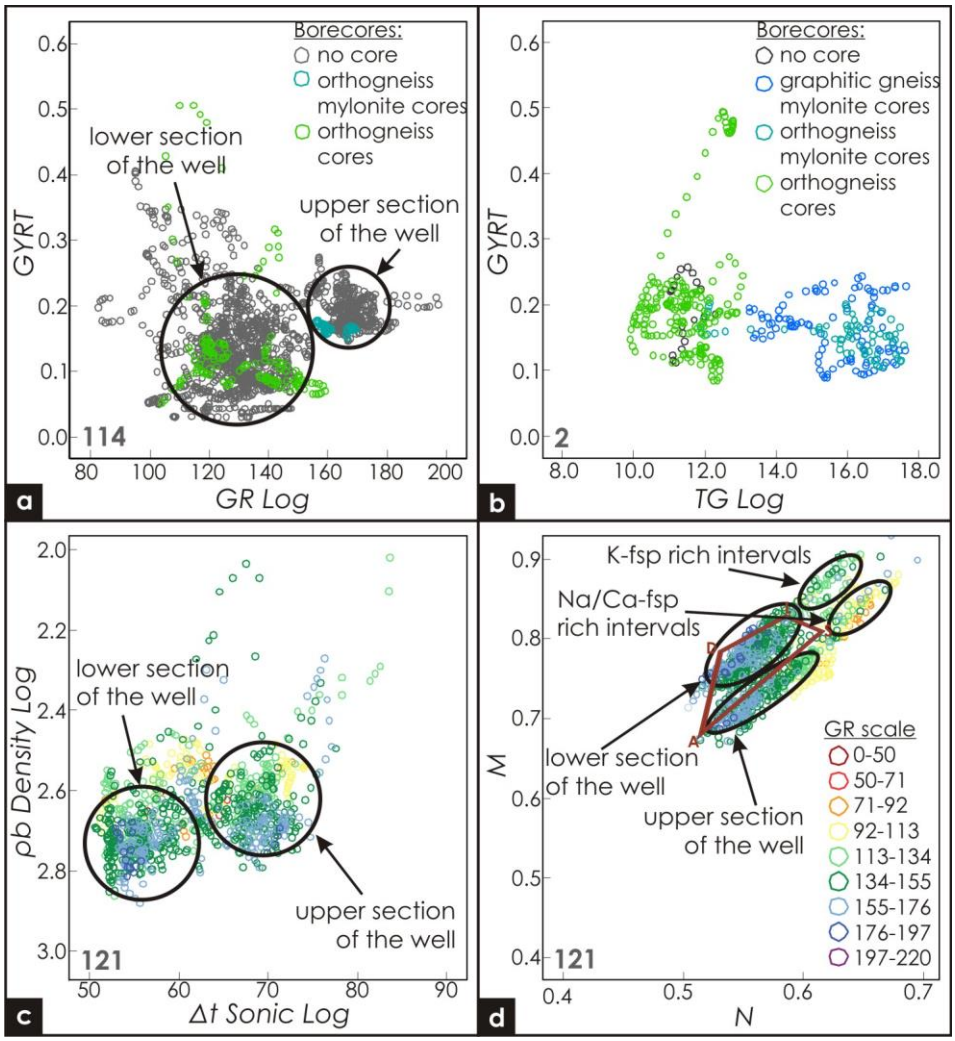

Figure 3. Plots of gneiss and mylonitic lithologies: a) Gamma-Resistivity plot of well-Q; b) Gamma-Resistivity log of well-J; c) Sonic – Density plot of well-F; d) MN plot of well-F. Legend: A – anhydrite, S – sandstone, L – limestone, D – dolomite.

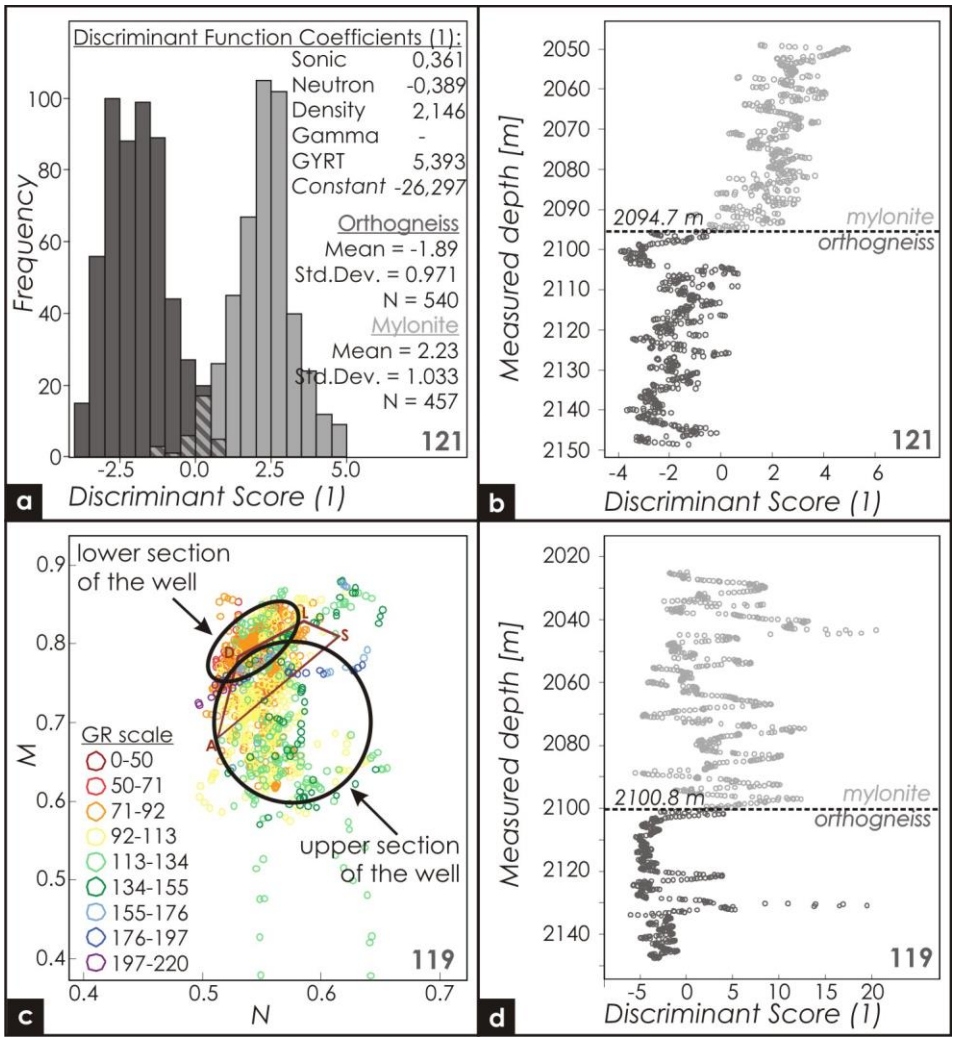

Figure 4. Discriminant function analysis (D1) of gneiss and mylonite with density, sonic, neutron logs: a) histogram of the discriminant scores (D1) of well-F; b) discriminant scores (D1) of well-F along the well; c) MN plot of well-119; d) discriminant scores (D1) of well-119 along the well.

Legend: A – anhydrite, S – sandstone, L – limestone, D - dolomite

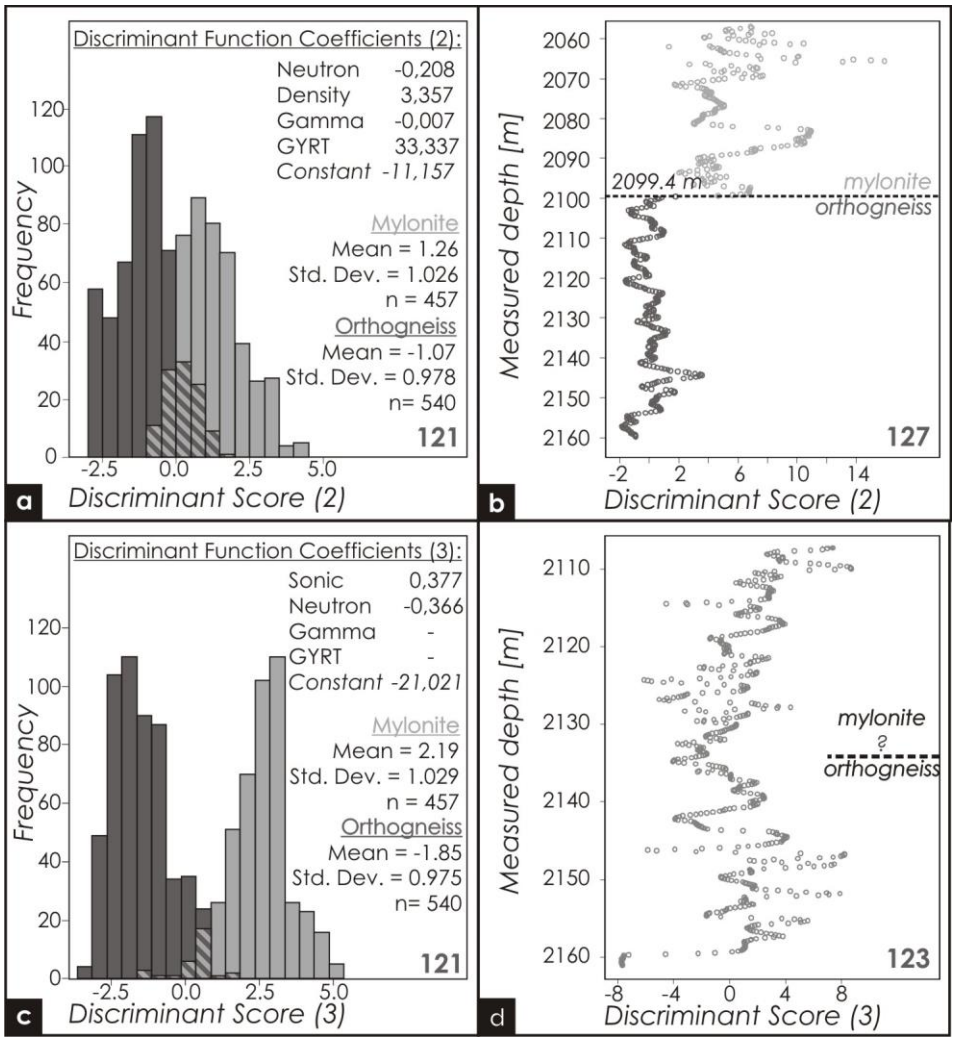

Figure 5. Discriminant function analysis (D2) of gneiss and mylonite with density and neutron logs: a) histogram of the discriminant scores (D2) of well-F; b) discriminant scores (D2) of well-N along the well. Discriminant function analysis (D3) of gneiss and mylonite with sonic and neutron logs: c) histogram of the discriminant score (D3) of well-F; d) discriminant scores of well-O along the well.

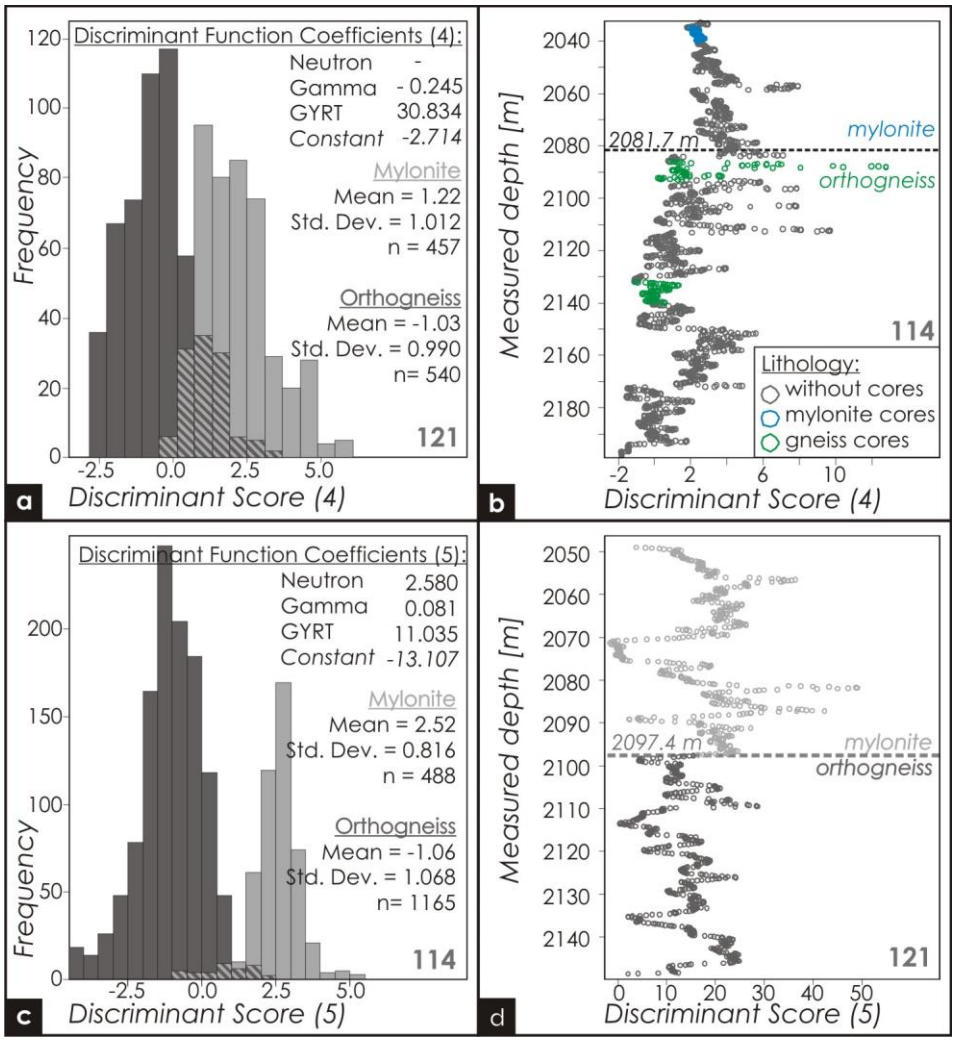

Figure 6. Discriminant function analysis (D4) of gneiss and mylonite with neutron: a) histogram of the discriminant scores of well-F; b) discriminant scores (D4) of well-Q along the well; c) histogram of the discriminant score (D5) of well-Q d) discriminant scores (D5) of well-F along the well.

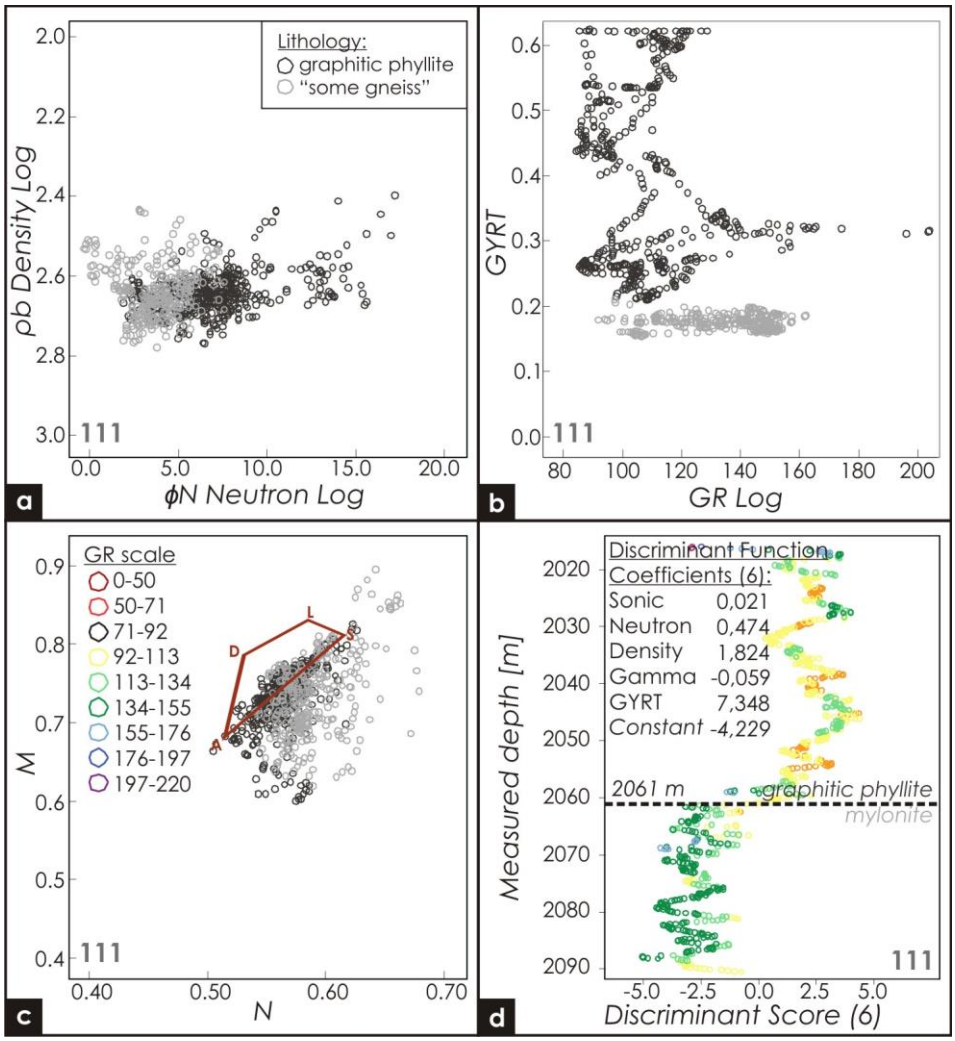

Figure 7. The a) neutron-density, the b) gamma-resistivity and the c) MN plot of the well-R; d) results of the discriminant function analysis (D6) for graphitic carbonate phyllite and mylonite in the well-R.

Legend: A – anhydrite, S – sandstone, L – limestone, D – dolomite.

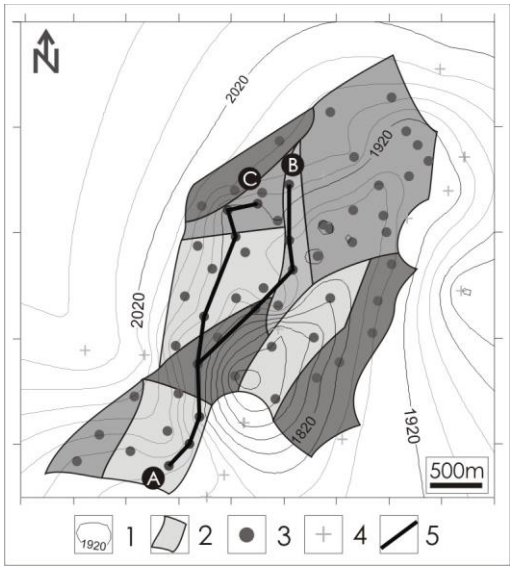

Figure 8. KIHA-NE wells situated on the metamorphic topography, with the ten hydraulic regimes and the lines of the geological sections of Figure 9.
Legend: 1 – counter lines of the metamorphic basement depth, 2 – hydraulic regime, 3 – well spot inside the reservoir, 4 – well spot outside the reservoir, 5 – lines of the geological sections.

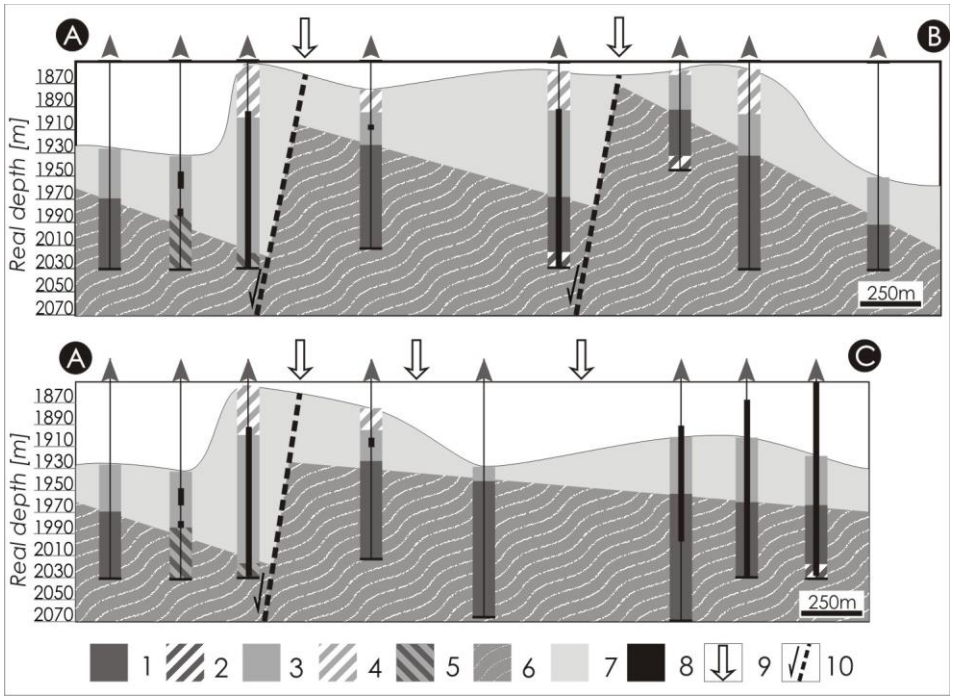

Figure 9. Geological sections through the field.
Legend: 1 – mylonite, 2 – probably mylonite, 3 – orthogneiss, 4 – probably orthogneiss, 5 – „some gneiss" (mylonite or gneiss) 6 – CH productive interval along the well; estimated 7 – mylonite or 8 – orthogneiss body; 9 – hydraulic regime boundary, 10 – assumed normal fault.

Table:

	Avaiable porosity logs				Discriminant fuction analysis					Plot	Lithology boundary
Well	**N**	**D**	**S**	**Core**	**N-D-S**	**N-D**	**N-S**	**N**	**N**	**GR-RT**	**lit**
A	#	#	#		OK						G / M
B	#	#	#		OK						G / M
C	#	#	#		OK						G / M
D	#	#	#		OK						G / M
E	#	#	#		OK						G / M
F	#	#	#		*D(1)*	*D(2)*	*D(3)*	*D(4)*	OK		G / M
G	#	#	#		OK						G / M
H	#	#	#		OK						G / M
I				#						X	M / M
J				#						OK - X	G/M/M
K	#	#				OK					G / M
L	#	#				OK					G / M
M	#	#				OK					G / M
N	#	#				OK					G / M
O	#		#				X				G / M
P	#		#				X				G / M
Q	#			#				OK	*D(5)*	OK	G / M
R	#	#	#		*D(6)*					OK	P / M
S				#						OK	P / M

Table 1. Summary of the used wells and results of them.

Legend: N – neutron log, D – density log, S – sonic log, D(1) – number of the discriminant function, OK – the discriminant analysis worked, X – the discriminant analysis did not worked, G/M – gneiss/mylonite lithology boundary, M/M – mylonite/mylonite lithology boundary, P/M – graphitic carbonate phyllite/mylonite lithology boundary.